Evaluating RTK GNSS-Assisted Close-Range Photogrammetry for Cultural Heritage Applications without GCPs

Wojciech Ostrowski [1,2], Kinga Wężka [3], Aleksandra Brzozowska-Jawornicka [4]

[1] Department of Photogrammetry, Remote Sensing and Spatial Information Systems, Faculty of Geodesy and Cartography, Warsaw University of Technology, Warsaw, Poland - wojciech.ostrowski@pw.edu.pl
[2] Institute of Archaeology, Jagiellonian University, Krakow, Poland
[3] Department of Geodesy and Geodetic Astronomy, Faculty of Geodesy and Cartography, Warsaw University of Technology, Warsaw, Poland - kinga.wezka@pw.edu.pl
[4] Department of History of Architecture, Art and Technology, Faculty of Architecture, Wrocław University of Science and Technology, Wrocław, Poland - aleksandra.brzozowska-jawornicka@pwr.edu.pl

Keywords: Exterior orientation, Georeferencing, GNSS-assisted photogrammetry, 3D Modelling, Cultural Heritage.

Abstract:

This study examines the potential of RTK GNSS-integrated close-range photogrammetry for documenting cultural heritage without the need for ground control points (GCPs). The research focuses on evaluating the GEOSTIX-X5 GNSS receiver, which enables direct synchronisation with a camera via the flash hot shoe, providing precise time-stamping of image capture events. The case study was conducted at Tomb 8 of the Tombs of the Kings in Paphos, a UNESCO World Heritage Site, and compares two datasets: a conventional photogrammetric survey from 2022 using GCPs and a 2025 survey employing GNSS-assisted photogrammetry. Both terrestrial and UAV imagery were acquired and processed in Agisoft Metashape, with accuracy assessment performed through cloud-to-cloud comparison in CloudCompare. Results indicate that the GNSS-integrated approach achieved single centimetre-level accuracy and no systematic scale errors. The findings demonstrate that RTK GNSS-assisted photogrammetry can significantly reduce fieldwork complexity while maintaining high accuracy, offering a promising alternative for heritage documentation where GCP placement is impractical or undesirable.

1. Introduction

The use of GNSS systems to determine camera positions within photogrammetric workflows is well established. For several decades, such techniques have constituted a fundamental component of both aerial and more recently UAV photogrammetry, where GNSS data have significantly enhanced the accuracy, efficiency, and automation of image-orientation procedures. In recent years, on-board RTK (survey grade) receivers have also become a key technological factor distinguishing consumer-grade drones from those intended for professional surveying. Consequently, the idea of extending GPS-assisted photogrammetry to close-range (terrestrial) applications appears entirely natural. The feasibility and accuracy of such an approach were investigated by Forlani et al. (2014), who integrated surveying-grade RTK receiver, receiving corrections from an NRTK service – based on a permanent GPS network, with a DSLR camera.

In subsequent years, attempts have been made to use similar solutions in various applications: shoreline change monitoring (Jaud et al., 2020), forest road surface deformation determination (Eker, 2023), as well as for cultural heritage applications (Eker et al., 2022; Oniga et al., 2024; Wieser et al., 2024). In the context of cultural heritage documentation – particularly with regard to 3D modelling of free-standing structures and buildings – the adoption of such solutions may enable the omission of ground control points (GCPs) during the photogrammetric processing stage. This is a significant advantage for the overall workflow, as the placement of control points on building façades requires measurements performed with a total station and the establishment of a dedicated survey network. These procedures are both time-consuming and operationally demanding, as they necessitate additional fieldwork and the transport and use of additional surveying equipment (total station).

Parallel research has also examined the feasibility of employing lower-accuracy GNSS receivers commonly integrated into mobile phones, which (by default) are tightly coupled with embedded cameras. However, the findings indicate notable limitations: insufficient positioning accuracy often leads to systematic horizontal and vertical shifts in the resulting 3D models (Jaud et al., 2020), while additional experiments have revealed scale instability when applying GNSS-aided photogrammetry based solely on smartphone-integrated sensors (Toriya et al., 2022). Nevertheless, survey-grade accuracy can be achieved when mobile phones are paired with external high-precision GNSS receivers, such as the Emlid RX used in conjunction with PIX4Dcatch processing workflows (Strecha et al., 2024)

Another solution that has emerged in recent years, based on miniaturised cameras, is the integration of cameras into GNSS-RTK receivers used by surveyors, such as Trimble or Leica. A detailed analysis of the Leica GS18i was presented by Peppa et al. (2024), who also show that using a DSLR camera and traditional photogrammetry with GCPs for the same objects provides better results, unsurprising given both the type of cameras installed inside GNSS receivers and the fact that these cameras are not intended for photogrammetric processing but rather for supplementing GNSS measurements with image-based measurements of hard-to-reach objects.

Published studies predominantly use two types of GNSS receivers: either large receivers intended for surveying (Forlani et al., 2014; Jaud et al., 2020; Oniga et al., 2024) from companies such as Leica, Trimble, or Topcon, or UAV-oriented receivers such as the Emlid Reach M2 (Eker et al., 2022; Eker, 2023; Oniga et al., 2024). An exception is the solution presented by Wieser et

https://doi.org/10.5194/isprs-archives-XLIX-B1-2026-315-2026

al. (2024), who developed a custom receiver designed for integration with a camera for terrestrial photogrammetry.

The primary objective of the presented research was to evaluate the GEOSTIX-X5 GNSS receiver, which can be directly connected to a camera via the flash sync port – hot shoe. This reciever was previously introduced by Mehdi Daakir and Aubin Bettiol (2025), who developed a stereo system (StereoBaseLine) based on two cameras coupled with two GNSS receivers and evaluated it in a challenging case study involving the inventory of linear infrastructure.

Therefore, the aim of this paper is to compare the results obtained using two different processing workflows applied to close-range photogrammetry and UAV imagery for cultural heritage documentation. The first workflow follows a classical approach based on an object-based control network measured using a total station, whereas the second workflow relies exclusively on camera position measurements acquired using RTK-based GNSS integrated with the camera via a hot-shoe connection.

2. Hardware and Study Area

2.1 Hardware

The GEOSTIX-X5 GNSS receiver is based on the Septentrio Mosaic-X5 GNSS module and provides the capability for external event time-stamping using the signal from the camera's hot shoe. It was connected with the Sony A7R III camera (Fig 1).

Figure 1. GEOSTIX-X5 GNSS receiver attached to Sony A7R III camera via the flash sync port (hot shoe).

The GEOSTIX-X5 receiver, incorporating the Septentrio mosaic-X5 GNSS module (GEOBSYS, 2026a), is designed for applications requiring high-precision positioning. The device supports tracking of signals from the GPS, GLONASS, Galileo, BeiDou, QZSS, SBAS, and L-Band systems on three frequencies, offering 448 channels and a positioning solution update rate of up to 100 Hz. The receiver is equipped with an integrated, multi-frequency helical antenna. It should be noted, however, that a complete antenna calibration model has not been made publicly available, which limits the ability to unambiguously assess the impact of the antenna's characteristics on the final positioning accuracy.

From the perspective of GNSS observations, helical antennas are generally considered advantageous due to their good compatibility with the circular polarization of satellite signals and their ability to effectively receive signals over a wide range of elevation angles (Maqsood et al., 2017). At the same time, practical GNSS measurements often exhibit lower stability in the vertical component compared to the horizontal component, which can be attributed to the effects of satellite constellation geometry, multipath phenomena, and variability in the antenna phase center position.

With regard to the receiver's accuracy performance, the analysis takes into account the results reported by Ferhat et al. (2025), according to which the GEOSTIX-X5 provides centimeter-level accuracy in the horizontal plane, while the vertical component remains significantly less accurate and requires further investigation. In the cited NRTK tests, horizontal differences with respect to reference points ranged from 1 to 4 cm, whereas vertical offsets of approximately 12–19 cm were observed.
For image geotagging purposes, the GEOSTIX-X5 receiver can be extended with the Hotshoe Layer module (GEOBSYS, 2026b), which is mounted in the standard hot-shoe of a photographic camera. Upon receiving the shutter release signal, the module records the image capture time with an accuracy better than 1 µs and subsequently stores the corresponding GNSS position. The version of the module used in the present measurements did not record the orientation of the camera–GEOSTIX system, which would otherwise be determined by the receiver's internal IMU.

This solution enables the integration of GNSS data with images already at the stage of field data acquisition; however, the accuracy of geotagging depends not only on the parameters of the receiver itself or GNSS observation conditions, the quality of available RTK/PPP corrections, but also the method of mounting the receiver relative to the camera, and the accurate determination of the geometric relationship (lever-arm, offset) between the antenna and the camera projection center.

Previous measurements of the study object were conducted in 2022 using a Canon EOS 6D camera, which was not equipped with a GNSS receiver; therefore, ground control points (GCPs) were used. In both measurement campaigns, the terrestrial images were complemented by a block of oblique UAV images. In 2022, the UAV data were acquired using a Phantom 4 RTK, whereas in 2025 a Mavic 3M RTK platform was employed. The detailed specifications of the cameras and UAV platforms used in both surveys are summarized in Table 1.

	2022	2025
Terrestrial Camera		
Model	Canon EOS 6D	Sony A7R III
Resolution	20 MP (5472 x 3648)	42.4 MP (7952 x 5304)
Pixel Size	6.6 µm	4.5 µm
Lens (f. length)	35 mm	35 mm
GNSS Receiver	no	GEOSTIX-X5
UAV		
Model	DJI Phantom 4 RTK	DJI Mavic 3M RTK
Resolution	20 MP (5280 x 3956)	20 MP (5280 x 3956)
Pixel Size	2.4 µm	3.3 µm
Lens (f. length)	8.8 mm	12.3 mm

Table 1. Parameters of cameras and drones used in the both surveys (2022 and 2025).

2.2 Study Area

Subject to detailed architectural investigation, the late Hellenistic Tomb 8 is situated within the "Tombs of the Kings" necropolis, located to the north of Nea Paphos in Cyprus, part of a UNESCO World Heritage Site.

Tomb 8 (Fig. 2) consists of an atypical rock-cut hypogeum of rectangular plan, with its longer axis oriented approximately east–west. The subterranean structure is organised into four orthogonal wings forming a circumambulatory passage around a central stone cube. Within this cube lies the principal burial niche, *Loculus* K. Opposite it is a monumental dromos providing access to the underground complex, composed of a flight of steps descending from ground level to a vestibule connected to the western wing of the passage. The central cube is additionally linked to the surrounding terrain *via* a stone passage situated above the eastern wing. Numerous burial niches, as well as two chambers, were carved into the walls and floor of the tomb (Hadjisavvas, 2025).

Figure 2. Aerial view of the study area: The Tomb 8 of the Paphos Tombs of the Kings.

In addition to the rock-cut hypogeum, Tomb 8 originally incorporated erected architectural structures. These, however, were destroyed in antiquity during an earthquake and have survived only as a dispersed assemblage of structural fragments and decorative architectural components.

Photogrammetric documentation of the monument enabled the accurate digital reconstruction of its form, which in turn facilitated detailed analysis of both the rock-cut fabric and the architectural elements. The latter, following comprehensive formal, stylistic, and structural examination, served as the basis for reconstructing the built components of Tomb 8 in the form of two richly decorated porticoes (Brzozowska-Jawornicka, 2025c) (Fig. 3), most likely erected during a second construction phase.

Figure 3. The porticoes of Tomb 8: reconstruction elaborated by A. Brzozowska-Jawornicka; visualisation by J. Michalik.

The first, referred to as the Western Portico, was positioned along the western face of the central cube within the western wing, directly opposite the dromos. It provided a monumental architectural setting for *Loculus* K, resembling a columnar temple façade crowned with a triangular pediment. The second, the Northern Portico, was constructed in front of the northern face of the core within the northern wing; in this instance, the colonnade was surmounted by a horizontal entablature.

It is noteworthy that, while the architectural decoration of both porticoes is firmly rooted in the Hellenistic tradition, it simultaneously demonstrates a high degree of innovation and originality (Brzozowska-Jawornicka, 2025a; Brzozowska-Jawornicka, 2025b).

3. Methods and Data Sets

3.1 Methods

Data from both surveys (2022 and 2025) were processed using Agisoft Metashape. In the first stage, image orientation was performed separately for terrestrial and UAV datasets in order to assess the internal accuracy and completeness of the aerial and ground image blocks. All four image datasets were successfully oriented without any issues. Following this initial verification, the terrestrial and UAV data were merged and oriented jointly in two separate processing workflows, one for the 2022 dataset and one for the 2025 dataset.

The workflow applied to the 2022 dataset followed a two-stage orientation strategy. In the first stage, the photographs were oriented using points measured with a total station in a local coordinate system; nine of these points were used as ground control points (GCPs) and six as check points (ChPs). In the second stage, the resulting model was transformed into a global reference frame using GNSS observations obtained from the UAV images. This processing approach was necessitated by difficulties in establishing a reliable connection to the GNSS reference network during the 2022 campaign. As a consequence, the GCP coordinates could only be determined in a local reference system, and the positioning accuracy of the UAV was lower than initially assumed.

For the 2025 dataset, the results of two different processing strategies were compared. The first approach, described by Eker et al. (2022), is based on performing image orientation without using camera position information and subsequently incorporating it only for later model rectification. In Agisoft Metashape, such a workflow can be implemented by importing GNSS observations for the images after the image alignment stage. A significant limitation of this approach, however, is that the GNSS observations do not directly participate in the bundle adjustment process, and consequently the offset between the GNSS antenna and the camera projection center is not estimated.

An alternative approach involves importing GNSS observations together with the images (prior to image alignment) or performing an additional self-calibration procedure that includes additional parameters for estimating the offset between the GNSS antenna and the camera projection center.

The final accuracy assessment was conducted in CloudCompare by directly comparing point clouds (calculating cloud-to-cloud distance), as the GCPs measured and used for model orientation in 2022 were marked (black-and-white checkerboards) and placed on the object only temporarily. Therefore, a direct comparison of GCP between the datasets was not possible. Moreover, due to the coarse georeferencing of the 2022 model, cloud-to-cloud alignment was applied (without scale adjustment).

3.2 Data Sets

Two image datasets (Tab. 2) were acquired during field campaigns conducted in 2022 and 2025 for the purposes of photogrammetric documentation and analysis.

Dataset		2022	2025
Images	Total	1885	1766
	Terrestrial	1518	1288
	UAV	367	478
Camera GNNS	UAV	RTK Float	RTK Fix
	Terrestrial	-	RTK Fix
Terrestrial reference		GCP (15)	-

Table 2. Parameters of data sets acquired during the 2022 and 2025 field campaigns.

The 2022 dataset comprises 1,885 images, including 1,518 terrestrial images and 367 images acquired using an unmanned aerial vehicle (UAV). During the UAV data acquisition in 2022, despite the use of an RTK-enabled GNSS receiver, it was not possible to obtain a fixed RTK positioning solution. The 2025 dataset consists of 1,766 images, of which 1,288 are terrestrial and 478 were acquired from the UAV platform. In contrast to the 2022 campaign, both UAV-based and terrestrial images (Fig. 4) acquired in 2025 achieved the expected positioning accuracy characteristic of RTK-class GNSS receivers.

All GNSS observations were conducted, similarly to the experiments reported by Forlani et al. (2014), using corrections provided by an NRTK service. The applied correction source was the national CORS network CYPOS—the primary permanent GNSS station network in Cyprus—which was established in 2008 and has since been operated by the Department of Lands and Surveys of the Ministry of the Interior (Danezis et al., 2020). The CYPOS system provides positioning results in the Cyprus Geodetic Reference System 1993 (CGRS93; EPSG:1112). This aspect requires particular attention during the import of UAV-derived observations, as Agisoft Metashape assigns WGS84 as the default reference coordinate system.

Additionally, in 2022, fifteen ground control points (GCPs) were measured using a total station; however, due to GNSS-related

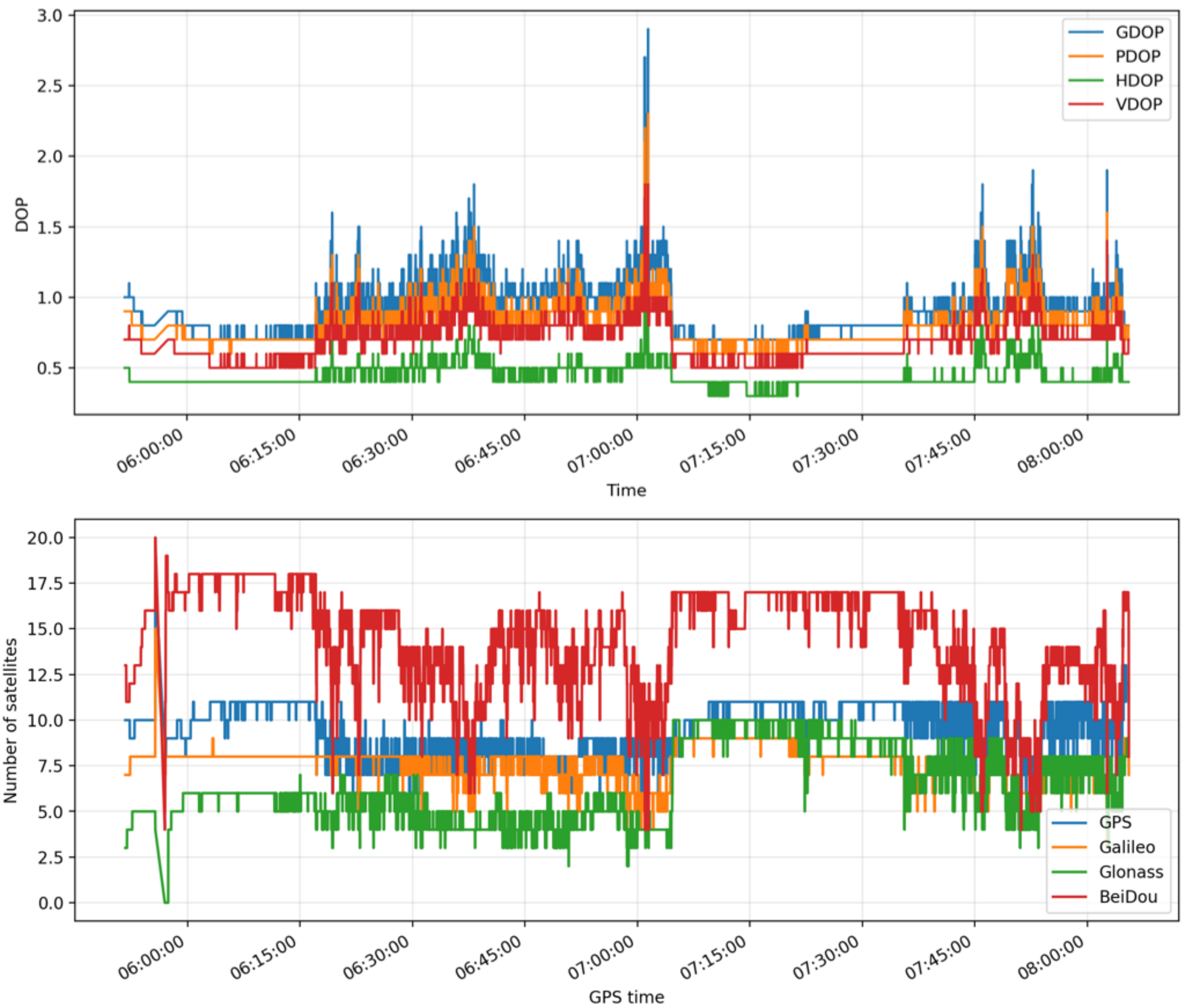

Figure 4. Variability of satellite visibility and dilution of precision (DOP) values for camera position determination using the GEOSTIX-X5 GNSS receiver during image acquisition in the 2025 survey.

issues, the coordinates of these markers were determined only within a local coordinate reference system. The GCPs established and measured during the 2022 campaign were no longer visible at the time of the 2025 survey.

4. Results

For the 2022 dataset, the accuracy (error) of image orientation (XYZ discrepancies of the projection centres) during aerotriangulation of the UAV images was approximately 40 cm. Consequently, the final model combining UAV and terrestrial images was generated using points measured with a total station in a local coordinate system (9 GCPs, RMSE = 1,5 cm) and validated using independent check points (6 ChPs, RMSE = 1,7 cm). GNSS observations from the UAV were therefore employed solely for coarse georeferencing of the model within a global coordinate reference frame.

The results of orienting the terrestrial images acquired in 2025 using a two-stage procedure (which did not include self-calibration with estimation of the lever-arm (offset) between antenna and camera) returned orientation errors (defined as differences between camera positions measured using GNSS and those estimated during aerotriangulation) at an RMSE level of approximately 6-7 cm in the horizontal plane (XY) and about 4 cm in the vertical component (Z). At the same time, the error distribution (Fig. 5) clearly indicates a systematic pattern, strongly correlated with the spatial orientation of the camera.

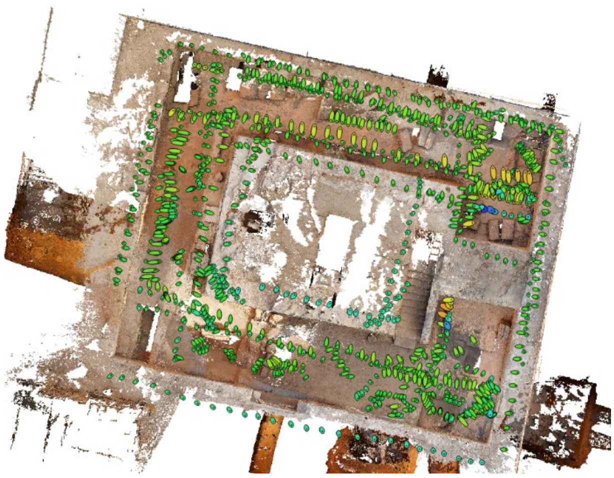

Figure 5. Spatial distribution of camera position errors for the dataset of terrestrial images acquired in 2025, resulting from the two-stage orientation – aerotriangulation performed without estimation of the offset (lever-arm) between the camera and the GNSS antenna.

A single-stage adjustment with simultaneous estimation of the offsets (lever-arm) resulted in substantially smaller orientation errors, amounting to 1.3-1.4 cm in the horizontal plane (XY) and 3.1 cm in the vertical component (Z), with no visible systematic effects (Fig. 6). The estimated offsets were -0.9 cm in the X direction, 20.6 cm in the Y direction, and 7.8 cm in the Z direction. It should be noted that the adopted camera coordinate convention assumes the Y-axis to be oriented upwards, i.e. toward the camera body in the direction of the hot-shoe mount.

A comparison of the point clouds generated from the two orientation strategies showed no horizontal displacement in the XY plane and no evidence of scale errors. However, a systematic vertical displacement in the Z direction is clearly visible (Fig. 7), amounting to approximately 21 cm. This offset is most likely attributable to the omission of the offset (lever-arm) between the camera projection center and the GNSS antenna during the orientation process.

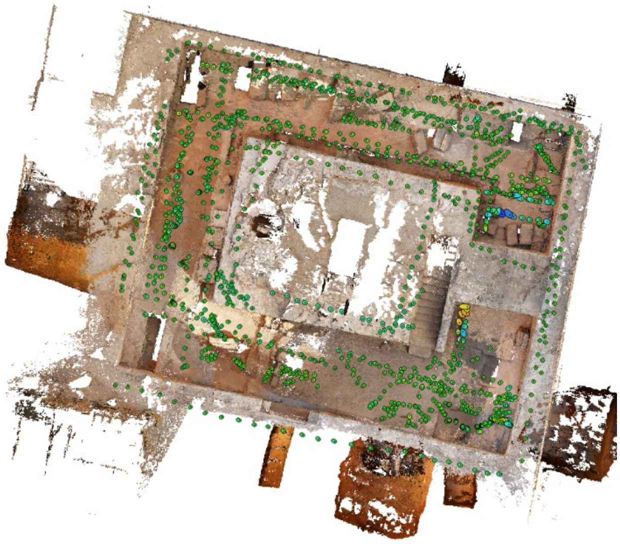

Figure 6. Spatial distribution of camera position errors for the dataset of terrestrial images acquired in 2025, resulting from the single-stage adjustment – aerotriangulation performed with estimation of the offset (lever-arm) between the camera and the GNSS antenna.

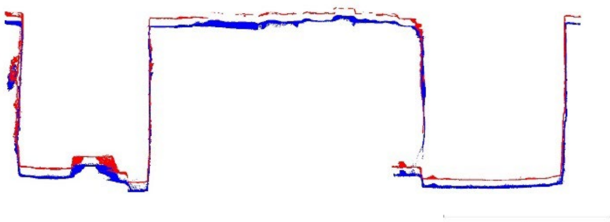

Figure 7. Cross-section through point clouds generated from terrestrial images (2025), obtained using a single-stage adjustment with lever-arm self-calibration (blue) and a two-stage adjustment without lever-arm self-calibration (red).

The joint adjustment of terrestrial and UAV images acquired in 2025 resulted in orientation errors (RMSE) comparable to those obtained for the single-stage adjustment, namely 1.4-1.7 cm in the horizontal plane (XY) and 2.9 cm in the vertical component (Z) of discrepancies for the projection centers. The estimated lever-arm offsets were also of similar magnitude to previous alignment, amounting to -1.0 cm in the X direction, 20.35 cm in the Y direction, and 7.7 cm in the Z direction. In addition, a bias term was estimated for the UAV-based GNSS observations within the adjustment, yielding values of -2.1 cm in X, -0.3 cm in Y, and 1.4 cm in Z.

The final comparison between the 2022 and 2025 models was conducted for the central part of the structure (Fig. 8). The comparison was carried out using a cloud-to-cloud distance analysis after applying cloud-to-cloud alignment (without scale adjustment) to the 2022 point cloud. The resulting distances revealed no systematic scale errors; however, minor discrepancies between the two models were observed, remaining within the accuracy range achieved for the check points (ChPs) in the 2022 dataset. The cloud-to-cloud analysis indicated that 68% of the points were within 1.1 cm, while 95% were within 2.7 cm. The mean offsets along the X, Y, and Z axes were effectively zero as a result of the prior cloud-to-cloud alignment procedure, with standard deviations ranging from 7 to 8 mm.

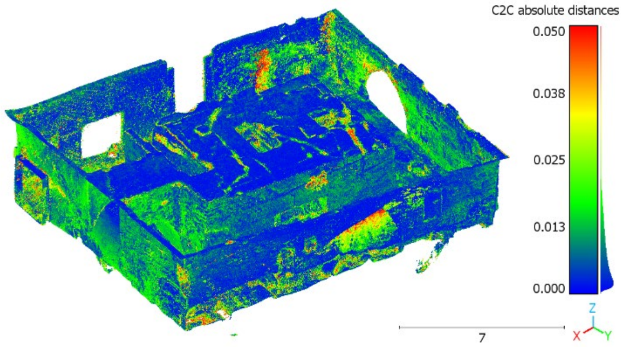

Figure 8. Cloud-to-cloud differences between final models from 2022 (generated using GCP) and 2025 (generated with RTK camera observations).

5. Conclusion

The results indicate that the GNSS-integrated approach achieved single-centimetre-level accuracy without introducing systematic scale errors. The conducted experiment, based on a direct comparison of two photogrammetric workflows for the documentation of a cultural heritage structure, clearly demonstrates the potential of modern GNSS-assisted solutions. The first workflow, applied during the 2022 survey, followed a classical methodology relying on ground control points (GCPs) measured with a total station in a local coordinate system and used for image orientation. The second workflow, tested using the 2025 dataset, was based exclusively on camera position measurements acquired with an RTK GNSS receiver integrated with the camera via a hot-shoe connection, without the use of any GCPs.

The comparative analysis shows that the RTK GNSS-based workflow can deliver results comparable to the classical GCP-based approach in terms of geometric accuracy, provided that the antenna–camera offset (lever-arm) is properly modelled and estimated during adjustment. At the same time, the GNSS-integrated approach significantly reduces fieldwork complexity by eliminating the need for establishing and measuring a local control network, which is often time-consuming, logistically demanding, and in some cases impractical or undesirable for heritage objects. Consequently, RTK GNSS-assisted photogrammetry represents a promising and efficient alternative for high-resolution cultural heritage documentation, particularly for free-standing structures and buildings where the placement of GCPs is limited by conservation, accessibility, or time constraints.

6. Acknowledgements

Research on Tomb 8 was conducted between 2023 and 2025 by an interdisciplinary team under lead of Aleksandra Brzozowska-Jawornicka (architect) at the invitation of Sophocles Hadjisavvas (archaeologist, Department of antiquities, Cyprus), director of the original excavations carried out between 1979 and 1981 (Hadjisavvas, 2012; Hadjisavvas, 2025). The project was funded by the National Science Centre Poland through the MINIATURA 6 grant (DEC-2022/06/X/HS3/01210), within the research programme In Search of the Hellenistic Architecture in Nea Paphos: Architectural Studies of Tomb 8 from the "Tombs of the Kings" Necropolis in the Wider Context of Hellenistic Funerary Architecture in the Eastern Mediterranean, as well as by the A. G. Leventis Foundation.

References

Brzozowska-Jawornicka, A. 2025a. *In Search of the Hellenistic Architecture in Nea Paphos: Architectural Studies of Tomb 8 from the "Tombs of the Kings" Necropolis in the Wider Context of Hellenistic Funerary Architecture in the Eastern Mediterranean* Online Catalogue. Repository for Open Data. https://repod.icm.edu.pl/dataset.xhtml?persistentId=doi:10.18150/RWXRNM (Accessed: 24 August 2025).

Brzozowska-Jawornicka, A. 2025b. Chapter 8. Architectural decoration from Tomb 8. In S. Hadjisavvas, *Tombs of the Kings: The Ptolemaic Necropolis of Pafos*, Vol. 1, *Excavation Seasons 1977-1981.* Lefkosia. Department of Antiquities.

Brzozowska-Jawornicka, A. 2025c. Chapter 9. The reconstruction of architectural structures from Tomb 8. In S. Hadjisavvas, *Tombs of the Kings: The Ptolemaic Necropolis of Pafos*, Vol. 1, *Excavation Seasons 1977-1981.* Lefkosia. Department of Antiquities.

Daakir, M., & Bettiol, A., 2025. StereoBaseLine: a flexible system for photogrammetric data acquisition in a linear configuration. *The International Archives of the Photogrammetry, Remote Sensing and Spatial Information Sciences*, *48*, 29-36. https://doi.org/10.5194/isprs-archives-XLVIII-1-W4-2025-29-2025

Danezis, C., Chatzinikos, M., & Kotsakis, C. 2020. Linear and Nonlinear Deformation Effects in the Permanent GNSS Network of Cyprus. *Sensors*, *20*(6), 1768.
https://doi.org/10.3390/s20061768

Eker, R., 2023. Comparative use of PPK-integrated close-range terrestrial photogrammetry and a handheld mobile laser scanner in the measurement of forest road surface deformation, *Measurement*, Volume 206, 2023, 112322, ISSN 0263-2241, https://doi.org/10.1016/j.measurement.2022.112322.

Eker, R., Elvanoglu, N., Ucar, Z., Bilici, E., & Aydın, A., 2022. 3D modelling of a historic windmill: PPK-aided terrestrial photogrammetry vs smartphone app. *The International Archives of the Photogrammetry, Remote Sensing and Spatial Information Sciences*, 43, 787-792. https://doi.org/10.5194/isprs-archives-XLIII-B2-2022-787-2022

Ferhat, G., Musq, I., & Ulrich, P., 2025. Evaluation of several GNSS receivers: from low-cost to high-end geodetic receivers. *6th Joint International Symposium on Deformation Monitoring (JISDM)*, Karlsruhe, Germany, 7–9 April 2025

Forlani, G., Pinto, L., Roncella, R, Pagliari, D., 2014. Terrestrial photogrammetry without ground control points. *Earth Sci Inform* **7**, 71–81 2014). https://doi.org/10.1007/s12145-013-0127-1

GEOBSYS, 2026a. GEOSTIX-X5 GNSS Receiver - Technical Specification. Available at:
https://www.geobsys.com/shop/geostix-x5-63 (22 March 2026).

GEOBSYS, 2026b. Hotshoe Layer Documentation - Description and Technical Data. Available at: https://docs.geobsys.com/en/layers/hotshoe/description/ (Accessed: 22 March 2026).

Hadjisavvas, S. 2012. *Digging up the Tombs of the Kings, a World Heritage Site*, NaPaphos Publishers, Nicosia 2012.

Hadjisavvas, S. 2025. *Tombs of the Kings: The Ptolemaic Necropolis of Pafos*, Vol. 1, *Excavation Seasons 1977-1981.* Lefkosia. Department of Antiquities.

Jaud, M., Bertin, S., Beauverger, M., Augereau, E., & Delacourt, C., 2020. RTK GNSS-Assisted Terrestrial SfM Photogrammetry without GCP: Application to Coastal Morphodynamics Monitoring. *Remote Sensing*, *12*(11), 1889. https://doi.org/10.3390/rs12111889

Maqsood, M., Gao, S., & Montenbruck, O., 2017. Antennas. In: Teunissen, P. J. G., & Montenbruck, O. (Eds.), *Springer Handbook of Global Navigation Satellite Systems*. Springer, Cham, 505-534. doi: 10.1007/978-3-319-42928-1_17.

Oniga, E., Boroianu, B., Morelli, L., Remondino, F., & Macovei, M., 2024. Beyond ground control points: cost-effective 3D building reconstruction through GNSS-integrated photogrammetry. *The International Archives of the Photogrammetry, Remote Sensing and Spatial Information Sciences*, *48*, 333-339. https://doi.org/10.5194/isprs-archives-XLVIII-2-W4-2024-333-2024

Peppa, M. V., Morelli, L., Remondino, F., & Mills, J. P., 2024. 3d geometric assessment of a commercial rtk/ppp visual positioning mobile sensor. *International Archives of the Photogrammetry, Remote Sensing and Spatial Information Sciences*, *48*, 97-104. https://doi.org/10.5194/isprs-archives-XLVIII-2-W7-2024-97-2024

Strecha, C., Rehak, M., & Cucci, D. 2024. The accuracy of RTK enabled mobile phones in RTK denied areas. ISPRS Annals of the Photogrammetry, Remote Sensing and Spatial Information Sciences, 10, 327-332. https://doi.org/10.5194/isprs-annals-X-4-2024-327-2024

Toriya, H., Tungol, Z. P. L., Ikeda, H., Owada, N., Jang, H. D., Adachi, T., ... & Kawamura, Y., 2022. Fragmentation size distribution measurement by GNSS-aided photogrammetry at real mine site. *Mining*, *2*(3), 438-448. https://doi.org/10.3390/mining2030023

Wieser, M., Verhoeven, G., Wild, B., & Pfeifer, N. 2024. Exterior Orientation in a Box: Cost-Effective RTK/IMU-Based Photo Geotagging. *The International Archives of the Photogrammetry, Remote Sensing and Spatial Information Sciences*, *48*, 463-470. https://doi.org/10.5194/isprs-archives-XLVIII-2-W8-2024-463-2024